Thermal Pressure in the Laser Heated Diamond Anvil Cell: A Quantitative Study and Implications for the Density vs. Mineralogy Correlation of the Mantle

Connor Ethan Yen[1),2)] Quentin Williams[3)] and Martin Kunz[1)]

[1)] Advanced Light Source, Lawrence Berkeley National Lab, 1 Cyclotron Rd, Berkeley CA 94720
[2)] Mathematics, University of California, Berkeley, CA 94720
[3)] Earth and Planetary Sciences, University of California, Santa Cruz, CA 95064

Keypoints:

laser-heated diamond anvil cell, thermal pressure, density – mineralogy correlation

Plain Language Summary:

The primary window into the interior of the Earth below ~10 km are earthquake waves that give us a 3-dimensional elasticity/density image of the planet. In order to translate this into a geological model of the Earth, we need to know the physical and chemical response of rocks with the composition of the Earth's interior at increased pressure and temperature. This is achieved by experiments in which samples are subjected to the high pressure and temperatures of the deep Earth using laser heated diamond anvil cells. A long standing problem of such experiments is a hard to quantify pressure term caused by the heating of the sample. This paper quantifies the thermal pressure distribution in a typical experiment for the first time and explores the effect of its incomplete knowledge on the possible mineralogical composition of the Earth.

Abstract:

We present the first quantitative measurements of the magnitude and gradient of thermal pressure in a laser heated diamond anvil cell (LHDAC). The observed thermal pressure is strongly localized and follows the distribution of the laser hotspot. The magnitude of the thermal pressure is of the order of the thermodynamic thermal pressure ($\alpha K_T \mathrm{d}T$) with gradients between 0.5 – 1.0 GPa/10 μm. This poses constraints on pressure determinations during PVT equation of state measurements when using a LHDAC. We show that an incomplete account of thermal pressure in PVT experiments can lead to distortions of the coveted depth versus mineralogy correlation. However, the ability to spatially resolve thermal pressure in a LHDAC opens avenues to measure thermodynamic derivative properties, which are important for comprehensive thermodynamic descriptions of the interior of planets.

1 Introduction

Over the past ~ 25 years, laser heated diamond anvil cells have played an important role in experimentally accessing the conditions of the interior of the Earth and Earth-sized planets (e.g. *Williams et al.* [1991]; *Guillaume Fiquet et al.* [1998]; *W Mao et al.* [2004]; *Ismailova et al.* [2016]; *Bassett* [2016]). The technique allows experimental simulation of pressures and temperatures relevant to the interior of the Earth, while allowing in-situ probing of structural and thermo-elastic properties of samples using a large portion of the electromagnetic spectrum (e.g. *Shen and Mao* [2016]; *Mezouar et al.* [2017]). Despite the maturity of this technique, there persist remarkable discrepancies between results reported from different experiments (e.g. *Komabayashi and Fei* [2010]), and also between experiments and theory (e.g. *Dorogokupets et al.* [2015]).

From an experimental angle, the sources of discrepancies in a LHDAC experiment are often associated with difficulties in measuring the pressure and temperature of the sample chamber. A second source of experimental uncertainty stems from the difficulty in positioning the probe (e.g. an X-ray beam) at a position of well-defined pressure and temperature within a sample volume with high thermal gradients (~10^4 K/mm) (e.g. *Panero and Jeanloz* [2001]; *Abby Kavner and Nugent* [2008]) and non-hydrostatic stress conditions (e.g. *Meng et al.* [1993]). Differences in sample preparation cause additional elements of limited reproducibility (e.g. *Marquardt and Marquardt* [2012]), as does unrecognized contamination (e.g. *Morard et al.* [2017]). An additional, and largely experimentally uncharacterized, contribution to measurement uncertainties in P-V-T experiments is the increase in pressure during the heating event due to quasi-isochoric conditions and the concomitant pressure increase and gradients induced by local heating. This effect is commonly referred to as thermal pressure (P_{th}); it is unrecorded in experimental set-ups where pressure is determined before and/or after the laser-heating event by using, for example, ruby fluorescence spectrometry. The combination of the laser heated material's finite shear strength and the temperature gradient produced by the focused laser spot produces a spatial gradient in thermal pressure which again is of the same order as the size of the probe.

The possible role of thermal pressure in laser-heated diamond cell experiments has long been recognized, but virtually no experiments have been conducted that measured the variation in thermal pressure *in situ* across a sample. In fact, the treatment of thermal pressure has been examined largely from a theoretical perspective. *Heinz* [1990] was the first to quantitatively address this issue from such a theoretical point of view. He estimated a P_{th} of ~ 2 - 10 GPa for a spherical Gaussian hot spot with T_{max} = 2000 K, a thermal expansivity α = 4 x 10 $^{-5}$/K, Poisson's ratio v = 0.25, and Young's modulus E = 200 GPa. These calculations were done for various ratios of hot-spot to sample size for two scenarios: the case of a free surface boundary condition (which implies constant pressure at the surface), and the case of a constant volume. Calculated values for P_{th} (~ 4 to 5 GPa) for small hot spot sizes were very similar in both scenarios, indicating a local nature of P_{th} with high pressure gradients associated with the laser-heated spot. This result implies that most of the thermal pressure is maintained via the shear strength of the heated material, rather than through the constant volume restriction provided by the metal gasket.

Dewaele et al. [1998] performed finite element modeling – also based on solving the thermoelastic equations – for a realistic LHDAC model assembly consisting of samples (stishovite and

coesite) sandwiched between an argon pressure medium. Their analysis included the effects of the thermal conductivity of the sample and pressure medium on the temperature distribution, as well as the effects of the bulk and shear moduli parameterized as Lamé constants. For both coesite and stishovite, they differentiated between a model with solid and liquid argon as the pressure medium. Their results for a solid pressure medium compare well with the results cited by *Heinz* [1990] –a thermal pressure increase of ~30 % of the 'cold' pressure. Interestingly, they found only a small dependence of the thermal pressure on the relative amount of solid argon used as pressure medium. Their second model, assuming a completely molten pressure medium, reduced the expected thermal pressure by about 50 %. This model approached the free-surface model of *Heinz* [1990].

G Fiquet et al. [1996], for the first time, reported direct observations of thermal pressure in a LHDAC while measuring P-V-T data of MgO periclase using a CO_2 laser. *Andrault et al.* [1998] experimentally determined the pressure increase induced by laser heating in a LHDAC using the phase transitions in the Mg_2SiO_4 and SiO_2 systems. They found that the observed increase relative to the perfectly isochoric 'thermodynamic' limit is sample dependent, correlating positively with the product of the thermal expansion and bulk modulus, αK_T (in accord with the ideal thermodynamic definition of thermal pressure as equal to $\alpha K_T \mathrm{d}T$), rather than with the shear modulus.

In this work, we experimentally quantify the distribution of thermal pressure created in a diamond anvil cell by a laser focus spot of 30 μm FWHM – a typical diameter of an experimental laser heating spot – and compare it with previously published models as well as a simple model based on the assumption of isochoric conditions. We then use an idealized example to quantify the effect of not fully taking into account the thermal pressure on thermoelastic properties of a mantle-like material ($Mg_{0.88}Fe_{0.12}SiO_3$ bridgmanite) extracted from a LHDAC experiment, and explore the implications for the resultant inferred mineralogy versus depth correlation.

2 Methods

We combine spatially resolved synchrotron X-ray powder diffraction [*Kunz et al.*, 2005; *Laugier and Bochu*, 2002; *Prescher and Prakapenka*, 2015] at distributed points along a BX90 [*Kantor et al.*, 2012] DAC's sample chamber's diameter with a 2-dimensional temperature map [*Kiefer and Duffy*, 2005; *Kunz et al.*, 2018; *Manga and Jeanloz*, 1996; *Rainey and Kavner*, 2014] of the sample chamber through pressure-volume-temperature (PVT) Murnaghan equation of states (EOS) [*Anderson*, 1997; *Angel et al.*, 2014; *Birch*, 1952; *Helffrich and Connolly*, 2009; *Murnaghan*, 1951] on samples of AgI [*Chauhan and Singh*, 2007; *Hull and Keen*, 1999] and San Carlos olivine [*Liu et al.*, 2005; *Liu and Li*, 2006] to determine the pressure distribution across the laser heated hotspot. By comparing these pressure values with the pressures measured at the same positions before the heating event [*H Mao et al.*, 1986], we obtain a distribution of the thermal pressure (P_{th}) produced by the heating event. More details on the sample and X-ray diffraction techniques, as well as on the laser heating and temperature mapping are given in the Supporting Information, Section 1.

3 Results

3.1 Temperature profiles

Figure 1 shows the temperature profile (red) across the hot spots in AgI and San Carlos olivine. The hot-spots can be fit with a Gaussian function (S.I. Table 1), and have approximately the width of the laser spot. These are in agreement with the Gaussian intensity distribution of the IR fiber laser, and indicate that the coupling of the samples with the laser is not markedly temperature dependent. Both temperature curves decrease to basically room temperature at the sample/gasket interface. This confirms the highly local nature of the temperature distribution in laser-heated samples within a DAC. It is therefore justified to assume that the cold gasket does not suffer any temperature-induced deformation: indeed, no irreversible deformation, as manifested by a shift in sample diameter, was observed following heating. The heating process of the entire sample volume is thus, to a first approximation, isochoric. To second order, it is possible that localized heating of the anvils may produce a slight contraction in the axial direction of the sample (even while the radial direction remains unchanged): the trade-off between the elastic response of the anvil to the thermal pressure within the sample and the thermal pressure induced by localized heating is difficult to characterize, but this effect is likely to be small.

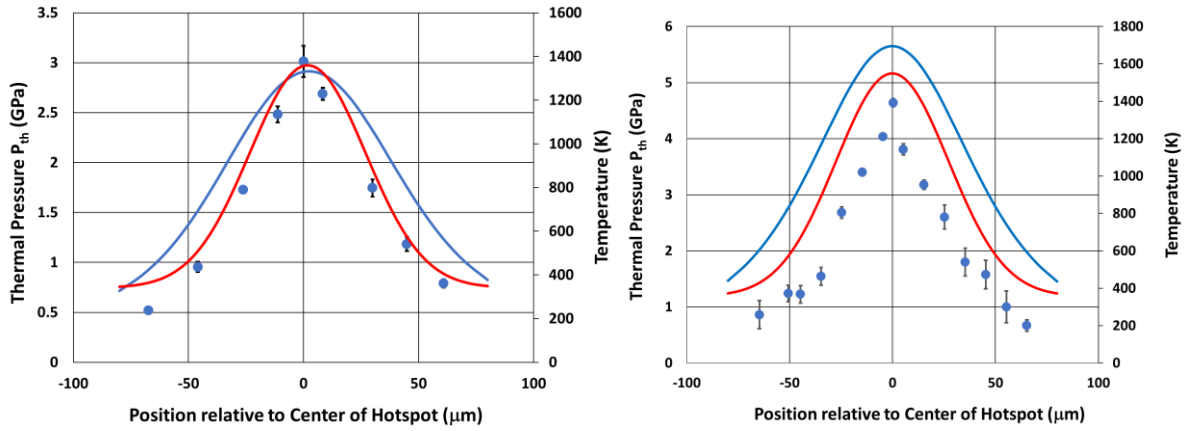

Figure 1: Observed beam temperature across the hotspot (red) and observed (blue symbols) and modeled (blue line) thermal pressure in AgI (a) and San Carlos olivine (b). The position of the pressure peak coincides with the hotspot peak as is expected for a thermal pressure-induced increase.

3.2 Pressure profiles

Figure 1 also shows the observed thermal pressure distribution (blue dots) across the laser heated hotspot (red line) as deduced from the procedure described above and in Supporting Information using the thermoelastic constants given in S.I. Table 1.

In both samples, a significant pressure peak, that is at the same location as the peak of the hotspot, is observed. In AgI, we observe a maximum thermal pressure of ~ 3 GPa at the center of the hotspot (~1400 K). It decreases to 0.5 GPa within about 70 μm. At the steepest part of the slope, about 20 μm from the center, the pressure drops by about 0.4 GPa per 10 μm. In San Carlos olivine, the situation is similar. A pronounced pressure maximum of ~4.5 GPa above the room-temperature value is measured

at the center of the hotspot (~1600 K). The thermal gradient is somewhat larger than in AgI, ~1 GPa/10 μm: this difference likely reflects the marked difference in strength between the two materials. It is notable, however, that even within a weak solid like AgI, the thermal pressure remains localized and does not fully re-equilibrate through viscous relaxation across the sample over the multi-minute course of the experiment.

Indeed, in both materials the thermal pressure distribution closely traces the temperature distribution, giving testament to the local nature of thermal pressure as predicted by *Dewaele et al.* [1998] and *Heinz* [1990]. Nevertheless, an effect that is plausibly associated with material strength can be experimentally discerned: the peak thermal pressure in AgI is slightly lower and the pressure distribution is wider than is observed in olivine.

4 Discussion

This is – to the best of our knowledge – the first documented experimental determination of the spatial distribution of thermal pressure across a laser heated spot within the diamond anvil cell. The general magnitude of the values reported here correspond quite well to the thermodynamic thermal pressure ($\alpha K_0 \, dT$) and also agree well with values predicted by *Heinz* [1990] for his constant volume model. That model corresponds closely to our experimental arrangement where a sample is loaded without pressure medium into a DAC and heated locally with a hot spot smaller than the sample volume. As expected, our values are somewhat higher (when adjusted for the hotspot's peak temperature) than the thermal pressures predicted by *Dewaele et al.* [1998] using finite element modeling. This is due to the fact that their modelling set-up included solid or liquid argon surrounding the sample as a pressure transmitting medium: such rare gas media are expected to be weak at high pressures (and temperatures), although argon can maintain substantial pressure gradients above ~20 GPa at 300 K [*Klotz et al.*, 2009].

The local nature of the observed thermal pressure is due to the finite shear strength of the expanding sample in a constrained volume. If the heated sample were a liquid or melt with no shear strength, the thermal pressure would equilibrate over the entire gasket hole. For the material, the size of the heated spot and sample, and the peak temperatures considered in this study, the equilibrated thermal pressure would amount to a homogeneous ~1.25 – 1.5 GPa increase across the entire sample volume. The observed gradients in thermal pressure therefore confirm that the temperatures attained were well below the melting point: however, even within a material that is expected to be relatively weak (AgI), thermal pressure-induced pressure increases of several GPa are observed.

To simulate the observed localized pressure increases within our samples, our model uses the non-zero shear strengths of the heated samples as a volumetric shielding mechanism between the colder material located radially outward from the hot spot, and the thermal expansion of the material within the hot spot (See Supporting Information Section 2). The volume of the heated material is therefore constrained to be smaller than the size of the gasket hole. We quantified this simple model by partitioning the sample volume with radial differential elements centered to the hot-spot. The temperature function was then derived from a Gaussian approximation of the experimental temperature maps. At a fixed radial distance, the thermal pressure is determined by assuming a rigid boundary at that fixed radial distance where the thermal expansion of the nested interior region is allowed to aggregate to a thermal pressure vector directed radially outwards. The fully rigid boundary construction assumed in our model is akin to

an infinite shear strength analogy that completely shields the colder exterior side of the shell from the hotter interior side. The model thus represents an upper bound on the expected thermal pressure increase. A detailed description of the model calculations is given in the Supporting Information, Section 2. The predicted pressure distributions of this simple model (blue curve) are compared with the experimental data (blue dots) in Figure 1. For AgI, the model predicts the peak pressure accurately, but under-estimates the pressure gradient. In the case of San Carlos olivine, the model predicts a pressure distribution that is shifted upward from the observed values by about 1 GPa (at an observed peak pressure of ~ 4.5 GPa). We attribute this discrepancy to the pressure gradient being too steep to be resolved with a 10 μm sized X-ray spot thus biasing the measured pressures towards lower values. This is consistent with the fact that the model matches the measured values much better for AgI where the lower shear strength allows for a flatter pressure gradient, which is better matched to the 10 μm X-ray spot size used. We therefore expect the real pressure increase to be sharper and to lie between the measured spots and the values given by the model.

Our measurements demonstrate that even for soft materials at temperatures close to their melting line, a significant pressure increase coupled with a pressure gradient around the localized hot spot is maintained in laser-heated diamond anvil cells. Given the steepness of the observed pressure gradient, this thermally-induced pressure increase and gradient is also expected to be significant in samples that are embedded in 'soft' pressure media such as Ne or He where their shear strength at high pressures becomes sufficient to contain the thermal pressure within the embedded sample (e.g. *Klotz et al.* [2009]). The shear strengths of the media consequently negate the full pressure-equilibrating effect expected in hydrostatic media for the pressure generated locally in the sample through local heating. These findings have ramifications for the design and interpretation of in-situ high-pressure high-temperature diffraction studies aimed at determining PVT equations of state of Earth materials and consequently for the mineralogical interpretation of geophysical density profiles based on LHDAC results.

Ramifications for LHDAC experimental designs:

(1) If, during a LHDAC experiment pressure is measured before and after the heating event, pressure can be significantly underestimated in the center of the hotspot (i.e. where the X-rays usually probe the sample) during the heating event: such localized, thermally-induced pressurization has not been previously characterized (e.g. *Andrault et al.* [1998]; *A Kavner and Duffy* [2001]).

(2) Pressure measurements using the diffraction lines of a temperature-insulating pressure medium (i.e. Ne, Ar, He) may similarly underestimate the pressure within the hot sample given the steep pressure gradients we observed within the hotspot. The underestimation of the pressure derived from the lattice parameters of a solid, non-laser-absorbing pressure medium (such as NaCl or MgO) could be larger if the pressure medium simultaneously also acts as a thermal insulation material shielding the diamonds from the laser hot spot. In that case, it is possible that a significant portion of the diffracting volume within the pressure medium is also at a temperature significantly below the peak temperature.

(3) As a consequence of (1) and (2), the most reliable pressure determination in a laser heated diamond anvil cell is likely generated by a pressure standard that is intimately mixed with the sample, monitored in situ at simultaneous high temperature and pressure, and which differs from the material used to thermally insulate the diamonds from the sample. Ideally, such an internal calibrant (often Pt) would also be chemically inert at extreme conditions in order to avoid unwanted chemical reaction or alloying with the sample. Such a mixed phase geometry can be particularly effective when deployed in

instances where the calibrant itself is used as the laser-absorber within the sample (e.g. *Tateno et al.* [2019]).

(4) The observed steep gradients in thermal pressure demonstrate that a straightforward means of experimental optimization, in terms of sampling a spot at well-constrained pressure and temperature, is to combine a large uniform hot spot (which can be generated using beam shaping optics, such as a Pi shaper) with the smallest possible X-ray probe. Naturally, a small X-ray beam has the inherent problem of reduced data quality due to a decrease in powder statistics. This is especially true at high temperatures where recrystallization and grain growth are often observed (e.g. [*Irifune et al.*, 2005] , [*Shen et al.*, 1998]). While poor powder diffraction statistics might still allow extraction of reliable volumetric data, other approaches could involve dispensing with monochromatic powder diffraction for PVT equation of state determinations based on diffraction. Single crystal and multigrain diffraction techniques are obvious alternatives that are commonly deployed at ambient temperatures, but are difficult (although not in principle impossible) to combine with laser heating, due to the requirement that the sample be rotated relative to the X-ray beam [*Dubrovinsky et al.*, 2010]. X-ray Laue microdiffraction can be a useful tool in cases where a sample cannot easily be rotated as required on a monochromatic single crystal diffractometer (e.g. *Barkov et al.* [2019]; *Tamura et al.* [2002]). However, in the absence of energy resolving area detectors, the application of Laue microdiffraction to PVT equation of state studies is not practical. A potentially viable technique that can be deployed using commonly available equipment is energy resolved Laue diffraction, which can use a scanning monochromator rather than an energy resolving detector. To make this approach feasible in the traditional transmission geometry employed in laser heating set-ups (e.g. *Kunz et al.* [2018], *Shen et al.* [2001]) requires a large energy range (~ 15 keV < E < 50 keV) to be covered in order to overcome the low density in reciprocal space coverage at low diffraction angles (e.g. *Kunz et al.* [2009]). Alternatively, a set-up where the laser heating is in the axial direction through the diamonds, but the detector is positioned at 90 degrees (i.e. signal through X-ray transparent gasket) could be envisaged.

The key point here is that the sharply peaked pressure distributions that we document within laser-heated spots motivate either smaller X-ray probes (and larger heated spots) than have previously been deployed, or alternate diffraction techniques to enhance the spatial resolution of the X-ray probe itself.

Ramifications for geophysical models derived based on LHDA experiments:

A systematic off-set in the assumed pressures for PVT equation of states, as would occur if part of the induced thermal pressure is not recognized, has consequences for the geophysical conclusions deduced from such experiments. As an example, we tested the effect on a hypothetical experiment on bridgmanite ($Mg_{(1-x)}Fe_xSiO_3$ (x = 0.12)). We created a synthetic PVT dataset with pre-heated pressures between ~25 and 100 GPa and 3 different mantle relevant temperatures (2000, 2500 and 3000 K), with imposed thermoelastic parameters (V_0, K_0, K', Anderson-Grüneisen δ, α_0, $d\alpha/dP$) derived from the literature and tabulated in Table 1. We add to the pre-heated pressure a thermal pressure of $\alpha K \Delta T$ (8.4, 10.9, 13.3 GPa), assuming an $\alpha K \sim 5 \times 10^{-3}$ GPa/K) in accordance with our measurements. We then use these synthetic V/V_0 – T data to fit a Murnaghan equation of state by assuming pressures that underestimated the total pressure by 2 GPa. This process yields a set of thermoelastic properties that are biased through the neglect of this thermal pressure (Table 1). As can be seen from Table 1, both the Anderson-Grüneisen parameter δ (dK/dT) and $d\alpha/dP$ refine towards values that predict a density vs pressure curve that is shifted positively (to higher densities) relative to the true values (Figure 2). If such

267 a slightly overestimated density vs depth (i.e. P and T) profile were compared with seismic data to
268 estimate the Fe content in bridgmanite in the Earth's mantle, this density difference would lead to an
269 underestimate of the Fe content in the mantle. For our model parameters, the sensitivity of the system
270 is such that even this small neglect of thermal pressure would generate an underestimate of the deep
271 mantle's inferred Fe number (based on a too-dense EOS) of ~0.03.

	"Synthetic" values	Refined values
V_0	163.7[1)]	Not refined
K_0	246.7[1)]	230.2(5)
K'	4.03[1)]	4.40(1)
Anderson-Grüneisen δ	3.25[2)]	1.74(6)
α_0	2.0×10^{-5} [3)]	$1.63(2) \times 10^{-5}$
dα/dP	-1.0×10^{-7} [3)]	$-1.01(2) \times 10^{-7}$

272

273 **Table 1: Thermoelastic parameters for the "synthetic" Bridgmanite that were used to create ideal V/Vo(P,T) values together**
274 **with the corresponding values obtained from fitting a Murnaghan equation against the same V/V0 and T but P points**
275 **underestimated by 2 GPa. See text for more details. 1) *Shukla et al.* [2016]; 2) The 'synthetic' δ is estimated by equating K(0)**
276 **+ dK/dT x ΔT = K0 x [1 + α(P) x Δ(T)]$^{-δ}$ and solving for δ. A dK/dT of ~ -0.01 is assumed for this [*Shukla et al.*, 2016]), α(P) is**
277 **assumed to be ~ 1.6 x 10^{-7} for this (*Wang et al.* [1994]. 3) *Utsumi et al.* [1995]**

278

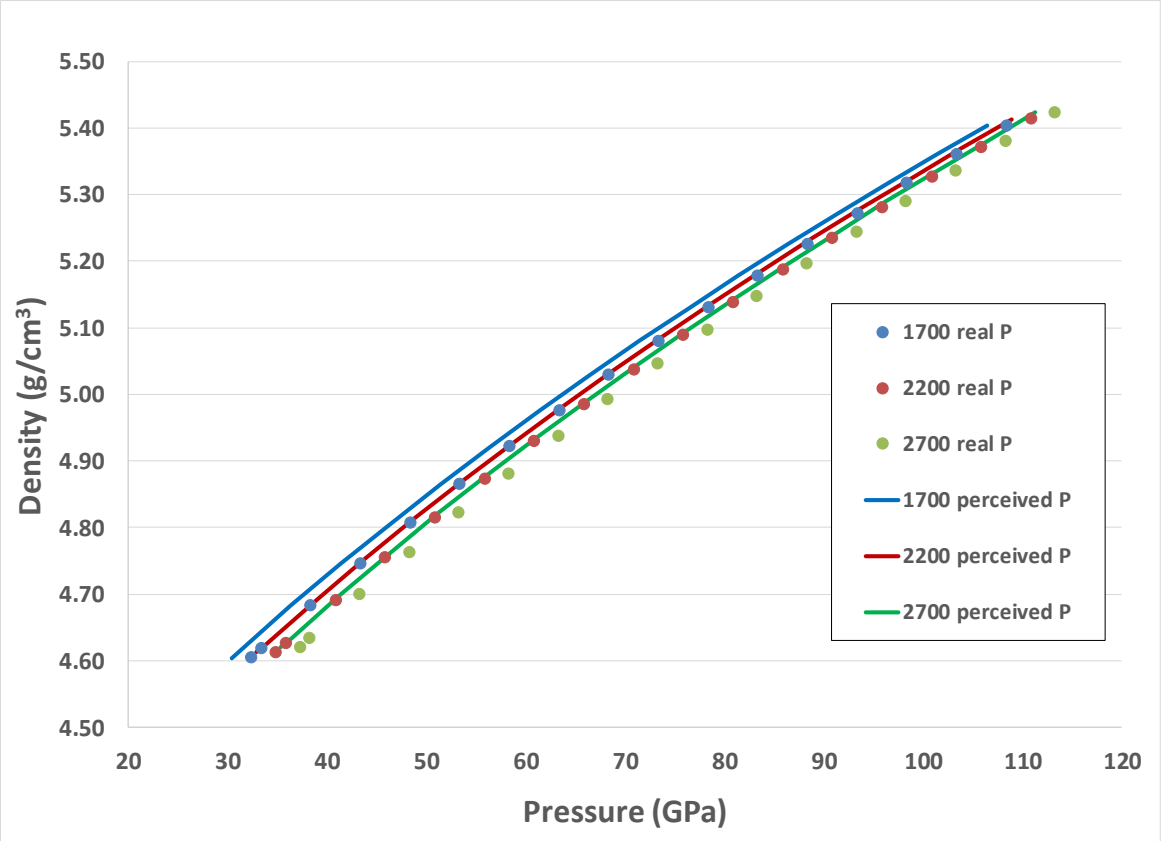

Figure 2: Density versus pressure values for synthetic ideal $(Mg_{0.88}Fe_{0.12})SiO_3$ bridgmanite at three different temperatures with thermal pressure contributions corresponding to $\alpha K_T dT$; and curves derived from thermoelastic properties as obtained from a PVT data set that underestimates the thermal pressure by 2 GPa ("perceived P"). This difference can for example lead to a wrong estimation of the Fe content of the phase considered (see text).

We note also that the local character of the thermal pressure elevations that we observe (Figure 1) suggests possible experimental avenues to measure difficult-to-characterize thermodynamic derivative properties. In particular, the sample translation techniques that we have documented can be deployed to measure the thermal pressure distributions within specially designed sample configurations. In particular, as shown in the Supporting Information Section 3, for a sample suspended in a medium that is of extremely high rigidity (e.g. diamond), the change in thermal pressure should reflect the thermodynamic value of $\alpha K_T \, dT$. As such, if the thermal pressure can be assessed at two (or more) different pressures at high temperatures, the thermodynamic relation of αK_T (at P,T) - αK_T (at P_0, T) being equal to the volumetric integral of $(\delta_T - K'_T)d\ln V$ can be deployed to provide a direct measure (assuming K' is constrained from equation of state measurements) of the Anderson-Grüneisen parameter at extreme conditions (e.g. *Anderson and Isaak* [1993]; *Jackson and Rigden* [1996]). The Anderson-Grüneisen parameter, which dictates the volume dependence of thermal expansion, is difficult to constrain at high pressures: it is inferred to decrease with compression, but its pressure dependence is not well known (*Anderson and Isaak* [1993]). In passing, we note that the other end-member, measurement of thermal pressure within a medium with zero strength (and high gasket strength), could also be deployed to constrain the pressure dependence of thermal pressure. In this instance, an accurate characterization of both the volume of the heated sample and of the sample chamber as a whole would be required to accurately interpret the sample-wide thermal pressure

increase. Hence, our present measurements demonstrate that, with appropriate experimental designs, accurate constraints on the pressure-dependence of the Anderson-Grüneisen parameter could be generated.

5 Conclusion:

We present the first quantitative experimental characterization of the pressure gradients caused by thermal pressures induced by temperature gradients in the laser-heated diamond anvil cell. The observed pressure increases correspond in magnitude to previously published theoretical and modeled values, and are also in accord with the thermodynamically expected value: the dominant parameter that governs the magnitude of thermal pressure is, unsurprisingly, the product of thermal expansion and the bulk modulus. Our results indicate that there is a nuanced effect on thermal pressure associated with material strength, thus showing that some diffusion of the stress field occurs within the samples. In particular, our results on AgI are both lower in their peak thermal pressure and have smaller spatial gradients of pressure with distance, which is consistent with AgI being weaker than olivine. Our simple modeling overestimates the thermal pressures accessed by olivine. We attribute this to the fact that the model provides an upper limit on the thermal pressure, combined with the fact that our X-ray probe is relatively large (10 μm) compared to the steepness of the pressure gradient (this is especially acute in olivine, where the observed pressure gradients are ~1 GPa/10 μm).

From an overarching perspective, our results clearly demonstrate that thermal pressures within laser-heated spots can be substantial and, even within relatively weak materials (AgI), remain localized around the laser-heated hot spot. As such, high-pressure/high-temperature measurements of (particularly) derivative parameters, such as thermal expansion at high pressures, likely require either multiple internal standards and/or a liquid medium to ensure that thermal expansions at extreme conditions are not underestimated. We also show that only a partial neglect of the thermal pressure can result in errors of the derived thermos-elastic properties that lead towards higher density at given P and T conditions. This in turns will cause significant errors on the correlation between density and mineralogy. Finally, our experimental design for measuring the spatial variations of thermal pressure could be deployed to quantitatively measure the pressure dependence of thermal pressure, and hence provide a direct constraint on the variation in the Anderson-Grüneisen parameter at deep planetary conditions.

Acknowledgments:

All raw data and analysis (diffraction images, temperature maps, pressure calculations, and density vs pressure analysis) are deposited in Dryad data repository (https://doi.org/10.7941/D1F63W).

X-ray diffraction experiments were performed at the Advanced Light Source (ALS) beamline 12.2.2. The ALS is supported by the Director, Office of Science, Office of Basic Energy Sciences, Materials Sciences Division, of the US Department of Energy under Contract No. DE-AC03-76SF00098 at the Lawrence Berkeley National Laboratory and the University of California, Berkeley. Sample preparation benefitted from the ALS laser mill purchased by the Consortium for Materials Properties Research in Earth Sciences;

339 COMPRES supported this project under the NSF Cooperative Agreement EAR 16-49658. QW is supported
340 by NSF EAR-1620423. EY was supported by a private fund (Yen-Zantua).

341 Discussions with Dion Heinz greatly improved this manuscript and are warmly acknowledged. A special
342 thanks is owed to Howard Padmore who not only helped fund this project, but also acted as a mentor
343 and source of inspiration.

References

Anderson, O. L. (1997), The volume dependence of thermal pressure in solids, *Journal of Physics and Chemistry of solids*, *58*(2), 335-343.

Anderson, O. L., and D. G. Isaak (1993), The dependence of the Anderson-Grüneisen parameter δT upon compression at extreme conditions, *Journal of Physics and Chemistry of Solids*, *54*(2), 221-227.

Andrault, D., G. Fiquet, J.-P. Itie, P. Richet, P. Gillet, D. Haeusermann, and M. Hanfland (1998), Thermal pressure in the laser-heated diamond-anvil cell; an X-ray diffraction study, *European Journal of Mineralogy*, *10*(5), 931-940.

Angel, R. J., M. Alvaro, and J. Gonzalez-Platas (2014), EosFit7c and a Fortran module (library) for equation of state calculations, *Zeitschrift für Kristallographie-Crystalline Materials*, *229*(5), 405-419.

Barkov, A. Y., L. Bindi, N. Tamura, G. I. Shvedov, B. Winkler, C. V. Stan, W. Morgenroth, R. F. Martin, F. Zaccarini, and C. J. Stanley (2019), Ognitite, NiBiTe, a new mineral species, and Co-rich maucherite from the Ognit ultramafic complex, Eastern Sayans, Russia, *Mineralogical Magazine*, *83*(5), 695-703.

Bassett, W. A. (2016), Diamond Anvil Cells: Laser Heating of Samples at High Pressure: 50 Years, *Laser Focus World*.

Birch, F. (1952), Elasticity and constitution of the Earth's interior, *Journal of Geophysical Research*, *57*(2), 227-286.

Chauhan, R., and C. Singh (2007), Equation of state and thermal expansivity of NaCl under high pressure and high temperature, *Physica B: Condensed Matter*, *387*(1-2), 352-357.

Dewaele, A., G. Fiquet, and P. Gillet (1998), Temperature and pressure distribution in the laser-heated diamond–anvil cell, *Review of scientific instruments*, *69*(6), 2421-2426.

Dorogokupets, P., A. Dymshits, T. Sokolova, B. Danilov, and K. Litasov (2015), The equations of state of forsterite, wadsleyite, ringwoodite, akimotoite, MgSiO3-perovskite, and postperovskite and phase diagram for the Mg2SiO4 system at pressures of up to 130 GPa, *Russian Geology and Geophysics*, *56*(1-2), 172-189.

Dubrovinsky, L., T. Boffa-Ballaran, K. Glazyrin, A. Kurnosov, D. Frost, M. Merlini, M. Hanfland, V. Prakapenka, P. Schouwink, and T. Pippinger (2010), Single-crystal X-ray diffraction at megabar pressures and temperatures of thousands of degrees, *High Pressure Research*, *30*(4), 620-633.

Fiquet, G., D. Andrault, A. Dewaele, T. Charpin, M. Kunz, and D. Haüsermann (1998), PVT equation of state of MgSiO3 perovskite, *Physics of the Earth and Planetary Interiors*, *105*(1-2), 21-31.

Fiquet, G., D. Andrault, J. Itie, P. Gillet, and P. Richet (1996), X-ray diffraction of periclase in a laser-heated diamond-anvil cell, *Physics of the Earth and Planetary Interiors*, *95*(1-2), 1-17.

Heinz, D. L. (1990), Thermal pressure in the laser-heated diamond anvil cell, *Geophysical Research Letters*, *17*(8), 1161-1164.

Helffrich, G., and J. Connolly (2009), Physical contradictions and remedies using simple polythermal equations of state, *American Mineralogist*, *94*(11-12), 1616-1619.

Hull, S., and D. Keen (1999), Pressure-induced phase transitions in AgCl, AgBr, and AgI, *Physical Review B*, *59*(2), 750.

Irifune, T., M. Isshiki, and S. Sakamoto (2005), Transmission electron microscope observation of the high-pressure form of magnesite retrieved from laser heated diamond anvil cell, *Earth and Planetary Science Letters*, *239*(1-2), 98-105.

Ismailova, L., E. Bykova, M. Bykov, V. Cerantola, C. McCammon, T. B. Ballaran, A. Bobrov, R. Sinmyo, N. Dubrovinskaia, and K. Glazyrin (2016), Stability of Fe, Al-bearing bridgmanite in the lower mantle and synthesis of pure Fe-bridgmanite, *Science advances*, *2*(7), e1600427.

Jackson, I., and S. M. Rigden (1996), Analysis of PVT data: constraints on the thermoelastic properties of high-pressure minerals, *Physics of the earth and planetary interiors*, *96*(2-3), 85-112.

Kantor, I., V. Prakapenka, A. Kantor, P. Dera, A. Kurnosov, S. Sinogeikin, N. Dubrovinskaia, and L. Dubrovinsky (2012), BX90: A new diamond anvil cell design for X-ray diffraction and optical measurements, *Review of Scientific Instruments*, *83*(12), 125102.

Kavner, A., and T. S. Duffy (2001), Strength and elasticity of ringwoodite at upper mantle pressures, *Geophysical Research Letters*, *28*(14), 2691-2694.

Kavner, A., and C. Nugent (2008), Precise measurements of radial temperature gradients in the laser-heated diamond anvil cell, *Review of Scientific Instruments*, *79*(2), 024902.

Kiefer, B., and T. S. Duffy (2005), Finite element simulations of the laser-heated diamond-anvil cell, *Journal of Applied Physics*, *97*(11), 114902.

Klotz, S., J. Chervin, P. Munsch, and G. Le Marchand (2009), Hydrostatic limits of 11 pressure transmitting media, *Journal of Physics D: Applied Physics*, *42*(7), 075413.

Komabayashi, T., and Y. Fei (2010), Internally consistent thermodynamic database for iron to the Earth's core conditions, *Journal of Geophysical Research: Solid Earth*, *115*(B3).

Kunz, M., A. A. MacDowell, W. A. Caldwell, D. Cambie, R. S. Celestre, E. E. Domning, R. M. Duarte, A. E. Gleason, J. M. Glossinger, and N. Kelez (2005), A beamline for high-pressure studies at the Advanced Light Source with a superconducting bending magnet as the source, *Journal of synchrotron radiation*, *12*(5), 650-658.

Kunz, M., N. Tamura, K. Chen, A. A. MacDowell, R. S. Celestre, M. M. Church, S. Fakra, E. E. Domning, J. M. Glossinger, and J. L. Kirschman (2009), A dedicated superbend X-ray microdiffraction beamline for materials, geo-, and environmental sciences at the advanced light source, *Review of Scientific Instruments*, *80*(3), 035108.

Kunz, M., J. Yan, E. Cornell, E. E. Domning, C. E. Yen, A. Doran, C. M. Beavers, A. Treger, Q. Williams, and A. A. MacDowell (2018), Implementation and application of the peak scaling method for temperature measurement in the laser heated diamond anvil cell, *Review of Scientific Instruments*, *89*(8), 083903.

Laugier, J., and B. Bochu (2002), CELREF V3: Cell parameters refinement program from powder diffraction diagram. Laboratoire des Matériaux et du Génie Physique, Institut National Polytechnique de Grenoble, France, edited.

Liu, W., J. Kung, and B. Li (2005), Elasticity of San Carlos olivine to 8 GPa and 1073 K, *Geophysical Research Letters*, *32*(16).

Liu, W., and B. Li (2006), Thermal equation of state of (Mg0. 9Fe0. 1) 2SiO4 olivine, *Physics of the Earth and Planetary Interiors*, *157*(3-4), 188-195.

Manga, M., and R. Jeanloz (1996), Axial temperature gradients in dielectric samples in the laser-heated diamond cell, *Geophysical research letters*, *23*(14), 1845-1848.

Mao, H., J.-A. Xu, and P. Bell (1986), Calibration of the ruby pressure gauge to 800 kbar under quasi-hydrostatic conditions, *Journal of Geophysical Research: Solid Earth*, *91*(B5), 4673-4676.

Mao, W., G. Shen, V. B. Prakapenka, Y. Meng, A. J. Campbell, D. L. Heinz, J. Shu, R. J. Hemley, and H.-K. Mao (2004), Ferromagnesian postperovskite silicates in the D ”layer of the Earth, *Proceedings of the National Academy of Sciences of the United States of America*, *101*(45), 15867-15869.

Marquardt, H., and K. Marquardt (2012), Focused ion beam preparation and characterization of single-crystal samples for high-pressure experiments in the diamond-anvil cell, *American Mineralogist*, *97*(2-3), 299-304.

Meng, Y., D. J. Weidner, and Y. Fei (1993), Deviatoric stress in a quasi-hydrostatic diamond anvil cell: Effect on the volume-based pressure calibration, *Geophysical Research Letters*, *20*(12), 1147-1150.

Mezouar, M., R. Giampaoli, G. Garbarino, I. Kantor, A. Dewaele, G. Weck, S. Boccato, V. Svitlyk, A. Rosa, and R. Torchio (2017), Methodology for in situ synchrotron X-ray studies in the laser-heated diamond anvil cell, *High Pressure Research*, *37*(2), 170-180.

Morard, G., D. Andrault, D. Antonangeli, Y. Nakajima, A. Auzende, E. Boulard, S. Cervera, A. Clark, O. Lord, and J. Siebert (2017), Fe–FeO and Fe–Fe3C melting relations at Earth's core–mantle boundary

conditions: Implications for a volatile-rich or oxygen-rich core, *Earth and Planetary Science Letters*, *473*, 94-103.
Murnaghan, F. D. (1951), *Finite deformation of an elastic solid*, John Wiley & Sons.
Panero, W., and R. Jeanloz (2001), Temperature gradients in the laser-heated diamond anvil cell, *Journal of Geophysical Research: Solid Earth*, *106*(B4), 6493-6498.
Prescher, C., and V. B. Prakapenka (2015), DIOPTAS: a program for reduction of two-dimensional X-ray diffraction data and data exploration, *High Pressure Research*, *35*(3), 223-230.
Rainey, E., and A. Kavner (2014), Peak scaling method to measure temperatures in the laser-heated diamond anvil cell and application to the thermal conductivity of MgO, *Journal of Geophysical Research: Solid Earth*, *119*(11), 8154-8170.
Shen, G., and H. K. Mao (2016), High-pressure studies with x-rays using diamond anvil cells, *Reports on Progress in Physics*, *80*(1), 016101.
Shen, G., H. k. Mao, R. J. Hemley, T. S. Duffy, and M. L. Rivers (1998), Melting and crystal structure of iron at high pressures and temperatures, *Geophysical Research Letters*, *25*(3), 373-376.
Shen, G., M. L. Rivers, Y. Wang, and S. R. Sutton (2001), Laser heated diamond cell system at the Advanced Photon Source for in situ X-ray measurements at high pressure and temperature, *Review of Scientific Instruments*, *72*(2), 1273-1282.
Shukla, G., M. Cococcioni, and R. M. Wentzcovitch (2016), Thermoelasticity of Fe3+-and Al-bearing bridgmanite: Effects of iron spin crossover, *Geophysical Research Letters*, *43*(11), 5661-5670.
Tamura, N., R. Celestre, A. MacDowell, H. Padmore, R. Spolenak, B. Valek, N. Meier Chang, A. Manceau, and J. Patel (2002), Submicron x-ray diffraction and its applications to problems in materials and environmental science, *Review of scientific instruments*, *73*(3), 1369-1372.
Tateno, S., T. Komabayashi, K. Hirose, N. Hirao, and Y. Ohishi (2019), Static compression of B2 KCl to 230 GPa and its PVT equation of state, *American Mineralogist*, *104*(5), 718-723.
Utsumi, W., N. Funamori, T. Yagi, E. Ito, T. Kikegawa, and O. Shimomura (1995), Thermal expansivity of MgSiO3 perovskite under high pressures up to 20 GPa, *Geophysical Research Letters*, *22*(9), 1005-1008.
Wang, Y., D. J. Weidner, R. C. Liebermann, and Y. Zhao (1994), PVT equation of state of (Mg, Fe) SiO3 perovskite: constraints on composition of the lower mantle, *Physics of the Earth and Planetary Interiors*, *83*(1), 13-40.
Williams, Q., E. Knittle, and R. Jeanloz (1991), The high-pressure melting curve of iron: A technical discussion, *Journal of Geophysical Research: Solid Earth*, *96*(B2), 2171-2184.

Figure 1a.

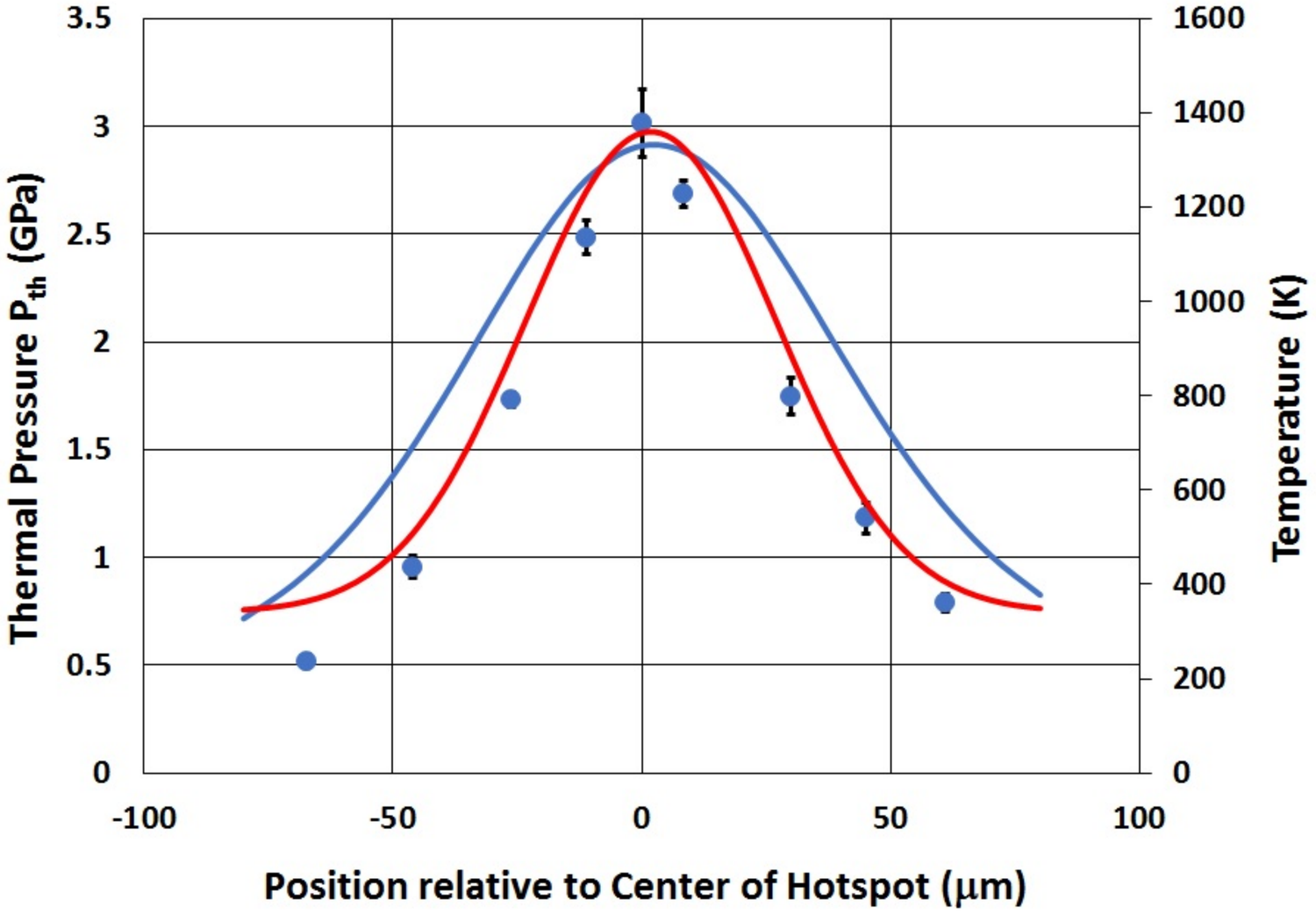
3.5
3
2.5
2
1.5
1
0.5
0
Thermal Pressure P_{th} (GPa)
1600
1400
1200
1000
800
600
400
200
0
Temperature (K)
-100
-50
0
50
100
Position relative to Center of Hotspot (μm)

Figure 1b.

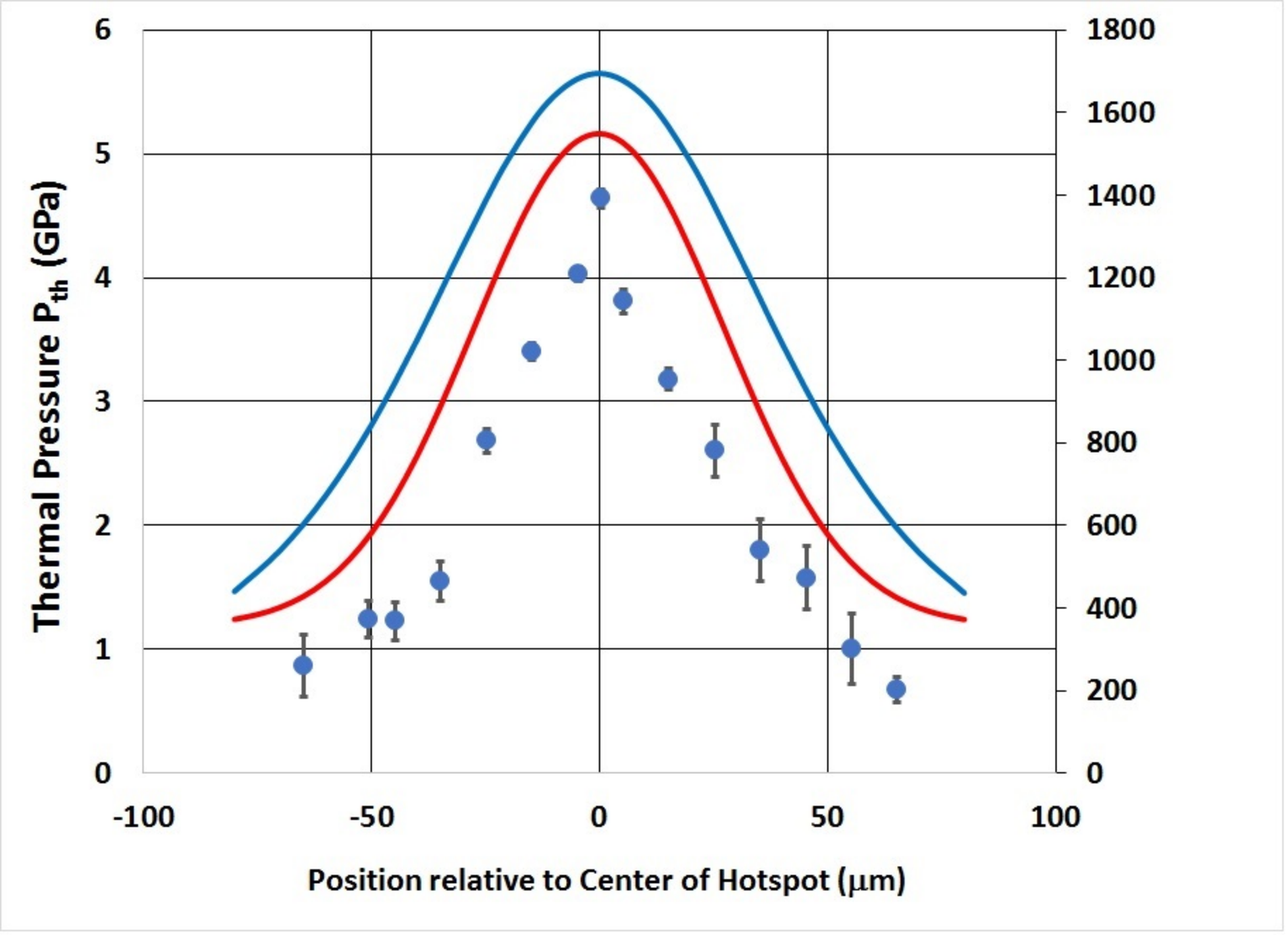
Thermal Pressure P_{th} (GPa)
6
5
4
3
2
1
0
1800
1600
1400
1200
1000
800
600
400
200
0
-100
-50
0
50
100
Position relative to Center of Hotspot (μm)

Figure 2.

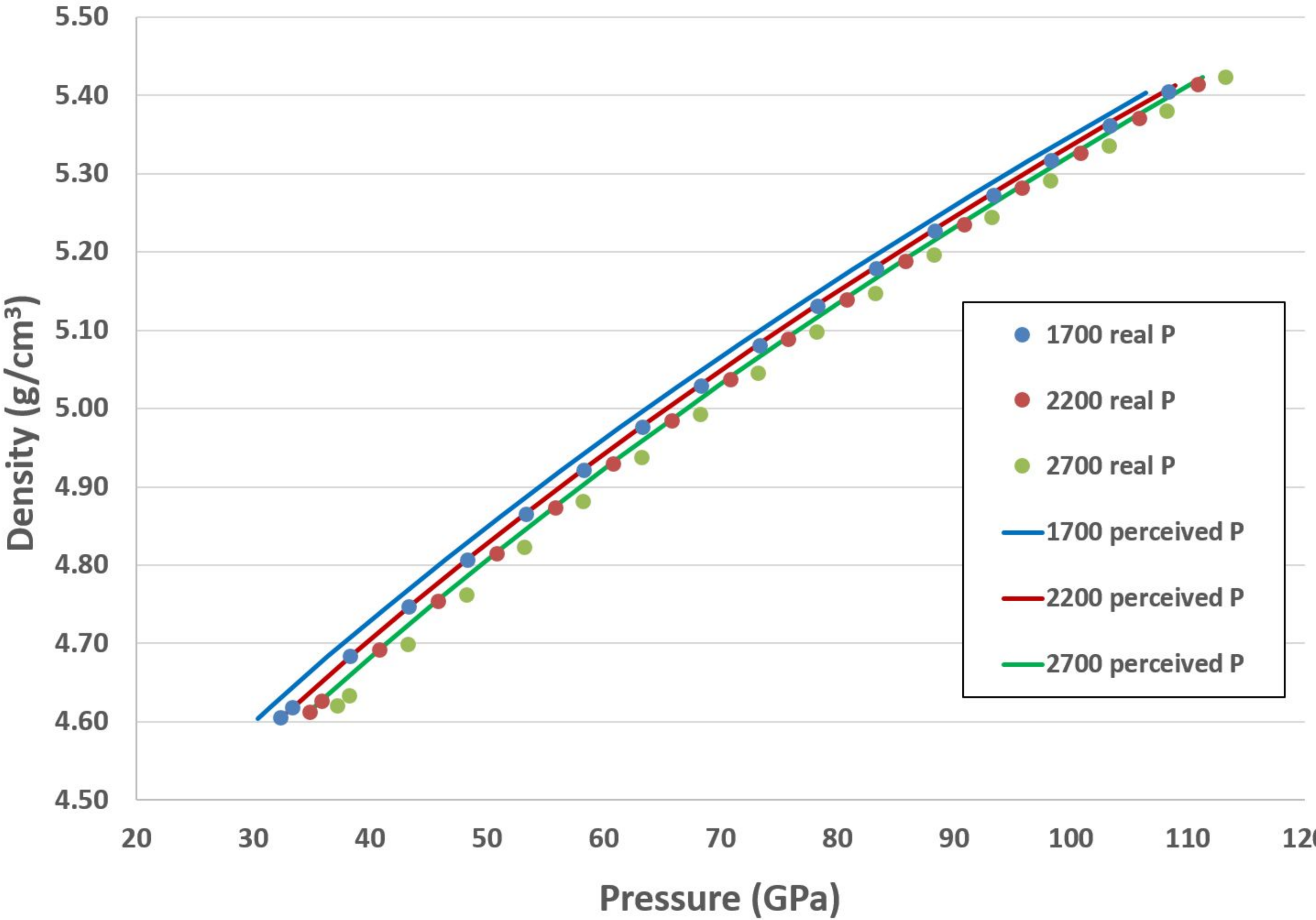
5.50
5.40
5.30
5.20
5.10
5.00
4.90
4.80
4.70
4.60
4.50
Density (g/cm³)
20
30
40
50
60
70
80
90
100
110
120
Pressure (GPa)
1700 real P
2200 real P
2700 real P
1700 perceived P
2200 perceived P
2700 perceived P